Towards the thermal management of electronic devices: A parametric investigation of finned heat sink filled with PCM

Adeel Arshad[a,*], Mohammed Ibrahim Alabdullatif[b,c], Mark Jabbal[a], Yuying Yan[a,*]

[a]*Fluids & Thermal Engineering (FLUTE) Research Group, Faculty of Engineering, University of Nottingham, Nottingham, NG7 2RD, United Kingdom*
[b]*Department of Mechanical Engineering, Faculty of Engineering, Islamic University of Madinah, Madinah, Saudi Arabia*
[c]*Department of Mechanical, Materials and Manufacturing Engineering, Faculty of Engineering, University of Nottingham, Nottingham, NG7 2RD, United Kingdom*

Abstract

This study presents the parametric investigation of a phase change material (PCM) filled plate-fin heat sink, used for thermal management (TM) of electronic components. Two-dimensional unsteady numerical simulations were carried out using the finite-volume-method. The plate-fin heat sink, which is acting as thermal conductivity enhancer (TCE), is employed with the PCM to improve the heat transfer enhancement. Two different volume fractions of 10% and 20% of plate-fin heat sinks with 10, 15 and 20 mm fin heights were selected and RT-35HC is used as PCM to absorb the internally generated heat by the electronic components. A constant input power, to mimic the electronic device heat generated, was provided at the heat sink base and transient variations of temperature distributions, melt-fraction, phase-change field, temperature flow field and latent-heat phase were analysed. The thermal performance of heat sinks was further investigated using dimensional analysis and critical set point temperature (SPTs). The results revealed that a PCM filled plate-fin heat sink reduced the heat sink base temperature and improved the uniformity of PCM melting compared with a without fins but PCM filled heat sink. The lower temperature of heat sink base was achieved with the increase of fin height and number of fins for both volume fractions of fins. Compared with the 10% volume fraction PCM filled finned heat sink, the 20 mm fin height of 20% volume fractions of fins showed better reduction in heat sink base temperature. However, the higher phase completion time during melting was predicted 20 mm fin height of 10% volume fraction of fins. A reduction in melting time is obtained

*Correspondence authors
Email addresses: adeel.arshad@nottingham.ac.uk, adeel_kirmani@hotmail.com (Adeel Arshad), yuying.yan@nottingham.ac.uk (Yuying Yan)

with higher fin height and number of fins.

Keywords: Plate-fin heat sinks, Phase change materials (PCMs), Thermal conductivity enhancers (TCEs), Thermal management, Electronic devices

Nomenclature

Abbreviations

FVM	Finite volume method
HS	Heat sink
TM	Thermal management
SPT	Set point temperature
PCM	Phase change material
TCE	Thermal conductivity enhancer

Symbols

A_m	Mushy zone
B	Boltzman constant (J/K)
ρc_p	Volumetric heat capacity ($J/m^3.K$)
g	Gravitational acceleration (m/s^2)
H	Height (mm)
k	Thermal conductivity ($W/m.K$)
L	Latent heat of fusion ($J/kg.K$)
m	Mass (kg)
p	Pressure (Pa)
S	Source term in momentum equation
V	Volume (m^3)
T	Temperature (K)
t	Time (sec)
u	Velocity component in $x-$axis (m/s)
v	Velocity component in $y-$axis (m/s)
W	Width (mm)
c_p	Specific heat capacity ($J/kg.K$)
ΔH	Fractional latent-heat ($J/kg.K$)
$2D$	Two dimensional

Greek letters

μ	Viscosity (Pa.s)
β	Thermal expansion coefficient (1/K)
f_l	Liquid fraction
γ	Volume fraction of TCE

Subscripts

ini	Initial
l	Liquidus
m	Melting
ref	Reference
x	$x-$axis
y	$y-$axis

1. Introduction

Thermal management (TM) methods for latest model of electronic devices have become increasingly important to stabilize the base temperature at desired level and guarantee essential features, such as reliability and user comfort. With advanced features of electronic packages, dissipation of an extra thermal load needs to be removed to prevent potential failure during the operation mode. Nearly 50% of failures in portable devices resulted from an increase in base temperature [1]. The conventional forced convection active cooling sources can improve the heat transfer rate, however such sources e.g. fans, heat exchangers, etc. are normally bulky volume, noisy, heavy weight, extra load consumption and periodic maintenance necessary, hence it is not suitable for the cooling of many modern electronic devices [2, 3].

Recently, passive TM of mobile devices employing the phase change materials (PCMs) and various therm conductivity enhancers (TCEs) such as metal-fins [4–6], metal-foams [7], metal-fibers [8, 9] and encapsulated PCMs [10] are employed to enhance the heat transfer rate because the PCMs exhibit the poor thermal conductivity results in transfer the poor heat flow from the heat source towards the ambient. These PCMs and TCEs based composite passive TM systems have been proposed as a novel approach for passive cooling of several applications, such as personal computers, hand-held phones, power electronic equipment, high-power lithium ion battery and aerospace engineering, to name a few [11–13]. PCMs are the best option for the cooling of electronic devices due to their high latent-heat of fusion at constant temperature and thermal and chemical stability [14]. The TCE namely finned heat sinks are mostly made of either copper or aluminium because of their higher thermal conductivity compared the PCMs. Therefore, the generated heat is uniformly dissipated throughout the sink unit. Further, resistance against corrosion and low density make these metals an appropriate choice for thermal management.

The PCMs are classified into three main categories namely, organic, inorganic and eutectic mixtures and have different functions based on their thermophysical properties. The organic paraffin-based PCMs are usually used due to their wide melting temperature range and consistent high latent-heat of fusion [15–17]. The employing of PCMs in heat sinks help in base temperature and heating rate reduction during an operation mode, hence enhancing device lifetime, durability, reliability and aid avoid potential failure [18]. PCMs have some notable characteristics, such as the ability to absorb/released heat at a constant temperature and high latent-heat of fusion, which provides major improvements in the cooling of electronic devices. For example, the PCMs have the capability to absorb/release a massive amount of energy while the device is in operation mode which is known as charging/discharging.

During the transition from a solid-to-liquid phase, PCM absorbs the heat and releases it again to the surrounding when the liquid is re-solidied [19]. The process of TM of electronic devices through the PCM/TCE technique can be divided into three major phases. Firstly, the PCM absorbs the released heat by an electronic device and the PCM temperature experiences a gradual increase to reach the melting point as pre-sensible heating. Secondly, PCM starts melting at a constant temperature. In this stage, latent-heat is absorbed with a slight change in volume that might happen ($< 10\%$) in the absence of temperature variation during the transition from solid-to-liquid phase as latent-heating phase. Finally, the temperature of liquid PCM increases again in the third phase as post-sensible heating [20]. PCMs can be utilised in many applications and purposes, such as air conditioning systems [21], aerospace applications [22], solar thermal application [23], water desalination [24], portable devices cooling [25, 26] and batteries [27].

Several studies have investigated the finned heat sink acting as a TCE embedded with the PCM. The influences of the PCM-based heat sinks, the arrangement and the optimum number of fins have been examined, experimentally, by Mahrous [28]. The heat sink was filled with the paraffin wax and the author found that the heating rate was decreased due to employed of PCM. Moreover, to improve cooling capability, Nayak et al. [29] performed the numerical study of a plate-fin and rod type PCM filled heat sinks of volume fraction of 5%, 10% and 15%. The results revealed that plate-fin PCM filled heat sink of 10% volume fraction had the best thermal performance. Arshad et al. [30] conducted an experimental investigation of pin-fin heat sinks filled with paraffin wax. The examined structural shape was the round pin type. The volumetric fractions of the PCM were chosen to be 0.0, 0.5 and 1.0 for both the with and without fins heat sinks. The results indicated that the volumetric fraction of 1.0 recorded superior thermal performance for both configurations and keeps the sink temperature within the desired range. Yazici et al. [31] experimentally studied the combined effects of fin angles and number of fins of a plate-fin heat sink filled with *n-eicosane*. The authors found the enhancement of 83.4% in operation time as the inclination angles 0 to 60 °C. In addition, the author found the best thermal performance at 60 °C and three number of fins based plate-fine heat sink. Xie et al. [32] conducted the numerical study using plate and tree-shaped finned heat sinks under with and without considering flow convection. The thermal behaviour of heat sinks revealed that natural convection heat transfer phenomenon exhibited the positive effects on thermal performance of PCM-based heat sink.

The selection of a suitable PCM is generally based on various aspects, such as high thermal conductivity, latent-heat of fusion and specific heat capacity, small change on its volume during phase transition and lower super-cooling. In addition, the melting temperature of a PCM should be lower than the maximum operating temperature of the electronic devices [33]. Nevertheless, it is quite essential to note that nearly all organic PCMs are suffering from a low thermal conductivity, which is an impediment to enhance the cooling performance. This issue increases the melting or cooling time of PCM and makes it quite difficult to employ heat storage capacity completely; such phenomenon is known as the self-insulating impact of the PCM. Thus, to increase the heat transfer rate of a chosen PCM, various configuration of extended surface geometries [34, 35] made from high thermal conductivity materials (TCMs) have been embedded with PCMs. The vast majority of numerical and experimental studies were conducted on the plate-fin type of heat sinks embedded with a PCM [36, 37]. Shatikian et al. [38, 39] numerically investigated the effect of fin length, thickness and spacing between two consecutive ns on the operating temperature. The results showed that the melting rate was enhanced as the distance between the fins was reduced. Pakrouh et al. [40] carried out a numerical study of a pin-fin heat sink filled with PCM and explored the heat sink base thickness, fin thickness and fin height, and number of fins. The finding indicated that number of fins had the significant impact in reduction of heat sink base temperature and then followed by heat sink thickness, height and base thickness. Hosseinizadeh et al. [41] presented both experimental and numerical investigation on PCM-based finned heat sinks to explore the impact of various TCEs. The considered heat sinks had constant dimensions and were embedded with RT-80 as the PCM. The authors proved that increasing the number of fins, fins height and the input power level can improve the overall thermal performance, whereas increasing the fin thickness had the lowest influence. From above aforementioned studies, the present numerical study investigates the effect of increasing fin height and volume fractions on the thermal performance of plate-fin heat sink. Three different fin heights of 10, 15, and 20 mm were considered having constant fin thickness of 2 mm. Three different volume fractions of plate-fins were chosen such as 0%, 10% and 20% to investigate the effect of number of fins. To achieve the safe and comfortable operating temperature range of 30-40 °C [13], the RT-35HC was filled inside the heat sink with melting temperature of 34-36 °C. The thermal performance of PCM-based finned heat sink then determined using different heat transfer performance factors such set point temperatures (STPs), average heat sink base temperature at a certain time period, and natural convective heat transfer enhancement was studied through dimensionless numbers. Finally, this study shall help to determine the appropriate fin height for thermal cooling of electronic devices.

2. Geometric and Mathematical description

2.1. Physics of the problem

In this study, the designed PCM-based finned heat sinks have a plate-fin structure acting as a TCE, which were numerically modelled to investigate the thermal capability at a constant heat flux input. The cross-sectional isometric view of heat sink having plate-fin metal structure and filled with PCM is shown in Fig. 1a for thermal management of electronic devices. A heat sink without fins filled with PCM was numerically explored as the reference heat sink for comparison purposes. The heat sinks were made of high conductive material, copper, for all proposed cases to guarantee their higher thermal conductivity, with three different volume fractions of TCEs 0%, 10% and 20%. The heat sink configurations were embedded with a PCM, namely, RT–35HC, which is a commercial grade of pure paraffin wax. The volume fraction (γ) of the TCEs was determined using Eq. 1, defined as the ratio of the total volume of the fins to total volume of the heat sink without fin [25]:

$$\gamma = \frac{V_{TCE}}{V_{HS}} \tag{1}$$

The design of the heat sink is based on the dimensions of the hand-held electronic devices to which it will be applied for thermal management. The overall dimensions are kept of $70 \times 70 \times 25$ mm^3 with 5 mm thickness of heat sink base and walls. All the surfaces of the heat sink are insulated to ensure the no heat loss across the boundaries during operation mode. The top surface of heat sink is covered with perspex sheet to visualize the melting/solidification process physically along with insulation of the surface. The conventional plate-fin was designed with 2 mm in thickness and a height of 10, 15 and 20 mm. The number of fins was calculated using Eq. 2. A constant heat flux of $q = 4000$ W/m^2 was applied uniformly from a heat source through the heat sink base. Fig. 2 presents the list of various plate-fin configurations investigated in this study. The physical domain and boundary conditions is known schematically in Fig. 1b. In this study, the two–dimensional ($2D$) geometry of all heat sinks is considered to have adiabatic walls. The dimensions of the physical domain, including finned heat sink are mentioned in Table 1. The thermophysical properties of RT–35HC, perspex sheet and copper are illustrated in Table 2 [42].

$$N_{fin} = \gamma \frac{V_{HS}}{V_{fin}} \tag{2}$$

2.2. Governing equations

A $2D$ analysis is modelled for the PCM–based heat sinks with plate–fin metal structure, as shown in Fig. 1b. The expressed governing equations are stated based on the problem in current study. The effect of phase change of the PCM embedded PCM inside the heat

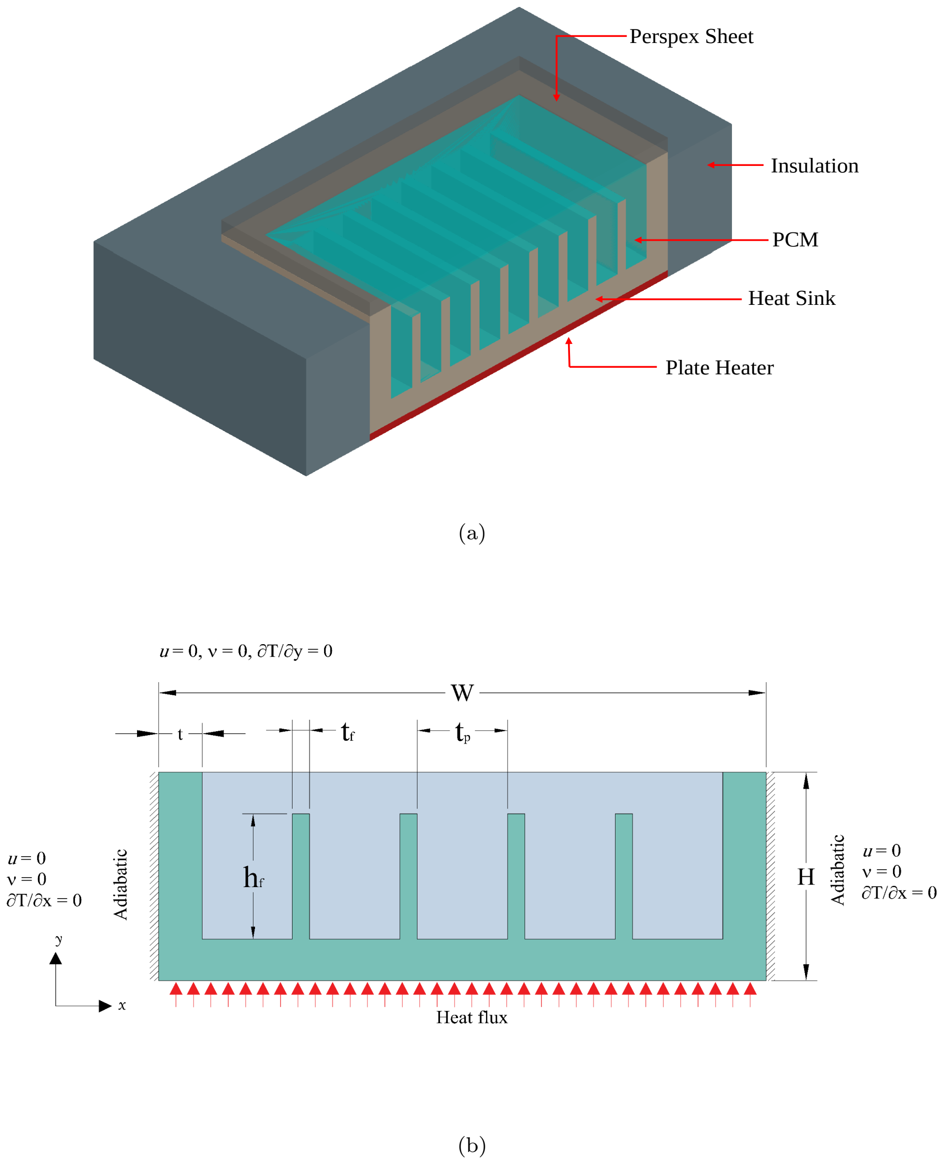

Figure 1: *(a) An isometric cross–sectional view of PCM filled finned heat sink assembly and (b) schematic diagram of the physical domain.*

Table 1: Dimensions of heat sinks.

Parameter	Dimensions (mm)
W	70
H	25
h_f	10, 15, 20
t_f	2

sink unit was captured using the enthalpy-porosity method. Furthermore, the proposed model of heat transfer was solved using continuity, momentum and energy equations. The melting/solidification model was considered due to the PCM phase–transition problem. Following the important assumptions are taken in consideration to simulate the current

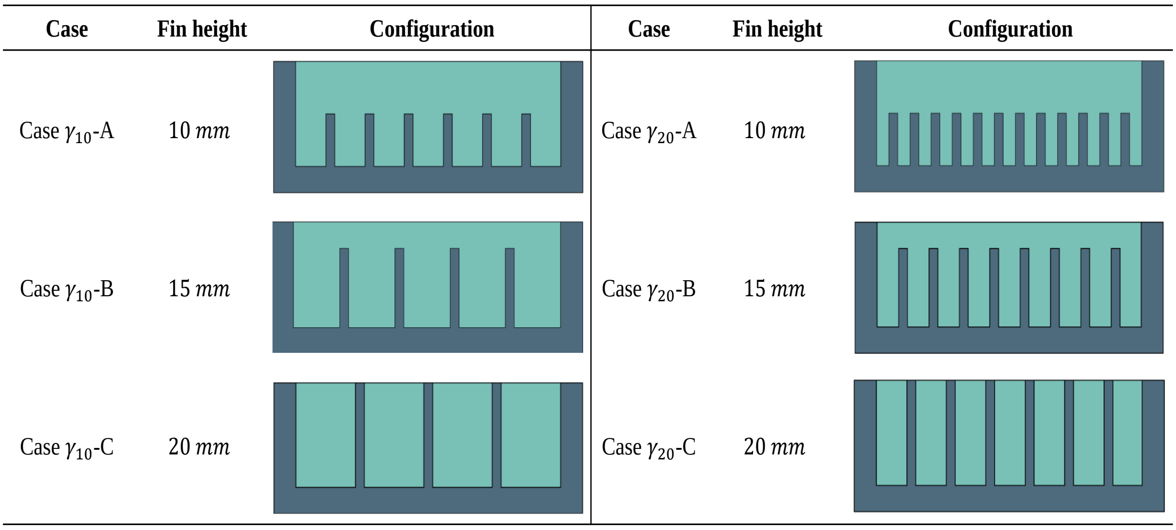

Figure 2: *Different plate-fin configurations investigated in this study.*

Table 2: Thermophysical properties of RT–35HC, perspex sheet and fins [43, 44].

Property	RT-35HC	Perspex sheet	Copper
T_m (K)	308.15	-	-
T_l (K)	309.5	-	-
T_s (K)	306.5	-	-
L (J/kg)	240,000	-	-
ρ (kg/m^3)	825	1180	8978
c_p (J/kg.K)	2000	1460	381
k (W/m.K)	0.2	0.186	387.6
β (1/K)	0.0006	-	-
μ (Pa.s)	0.0235	-	-

problem [14, 39, 45]:

- The heat sink and the PCM are at the melting temperature point of the PCM.
- The heat sink always remains in a solid state and only sensible heat is absorbed.
- The material of heat sink is homogeneous and isotropic.
- The liquid PCM is assumed to be incompressible Newtonian fluid, laminar and under unsteady state; it is subjected to Boussinesq approximation.
- Local thermal equilibrium exists between the fins and liquid PCM.
- The thermophysical properties of the PCM and heat sink are assumed to be constant over the temperature and phase range.

- The volume change of the PCM is neglected during the phase–transition of melting and solidification.

Accordingly, based on the above-mentioned assumptions, the governing conservation equations for mass, momentum and energy can be expressed as follows [44, 46, 47]:

Mass conservation:

$$\frac{\partial u}{\partial x} + \frac{\partial v}{\partial y} = 0 \tag{3}$$

Momentum conservation:

$$\rho\left(\frac{\partial u}{\partial t} + u\frac{\partial u}{\partial x} + v\frac{\partial u}{\partial y}\right) = -\frac{\partial p}{\partial x} + \mu\left(\frac{\partial^2 u}{\partial x^2} + \frac{\partial^2 u}{\partial y^2}\right) + S_x \tag{4}$$

$$\rho\left(\frac{\partial v}{\partial t} + u\frac{\partial v}{\partial x} + v\frac{\partial v}{\partial y}\right) = -\frac{\partial p}{\partial y} + \mu\left(\frac{\partial^2 v}{\partial x^2} + \frac{\partial^2 v}{\partial y^2}\right) + \rho_{ref} g\beta(T - T_{ref}) + S_y \tag{5}$$

Energy conservation:

$$(\rho c_p)\left(\frac{\partial T}{\partial t} + u\frac{\partial T}{\partial x} + v\frac{\partial T}{\partial y}\right) = k\left(\frac{\partial^2 T}{\partial x^2} + \frac{\partial^2 T}{\partial y^2}\right) + S_h \tag{6}$$

Where, the u and v are the rate velocity components in x and y directions, respectively, ρ is the density (kg/m^3), t is the time (s), p is the pressure (Pa), g is the gravitational body acceleration (m/s^2), μ is the dynamic viscosity $(kg/m.s)$, ρc_p is the thermal capacitance and k is the thermal conductivity $(W/m.K)$. The thermal expansion coefficient of the material, β, has a value of $\beta = 0.0006\ K^{-1}$. The S_x and S_y terms in the momentum Eqs. 4 and 5 are the source terms (N/m^3) which are associated with the change in porosity in mushy–zone and can be written as follows:

$$S_x = -A_{mush}\frac{(1-f_l)^2}{f_l^3 - \varepsilon}.u \qquad S_y = -A_{mush}\frac{(1-f_l)^2}{f_l^3 - \varepsilon}.v \tag{7}$$

Where, A_{mush} is a constant number (10^5) that illustrates the morphology of the mushy zone [14] and $\varepsilon = 0.001$ is only a constant value applied to avoid divide by zero. Moreover, f_l is the liquid fraction of the PCM in the mushy region, and can be defined as:

$$f_l = \frac{\Delta H}{L} = \begin{cases} 0 & \text{if } T < T_s \\ \frac{T-T_s}{T_l-T_s} & \text{if } T_s < T < T_l \\ 1 & \text{if } T > T_l \end{cases} \tag{8}$$

Where, T, T_s and T_l are the average temperature, solidus temperature and liquidus temperature of the PCM, respectively. The total enthalpy (H), the sum of sensible and latent–heat of enthalpies, can be defined as follows:

$$H = \Delta H + h \tag{9}$$

Where, ΔH and h are the fractional latent–heat ans sensible heat of enthalpies of the PCM and and are defined by:

$$\Delta H = f_l L \tag{10}$$

$$h = h_{ref} + \int_{T_{ref}}^{T} c_p dT \tag{11}$$

Where, h_{ref} is the reference enthalpy, T_{ref} is the reference temperature, c_p is the specific heat and L is the latent–heat of fusion for between 0 for solid and L for liquid. Further, the S_h term in the energy Eq. 6 describes the latent–heat storage due to the melting of the PCM and is defined by:

$$S_h = -\frac{\partial(\rho \Delta H)}{\partial t} \tag{12}$$

Where,

$$\Delta H = \begin{cases} 0 & \text{if } T < T_m \\ f_l L & \text{if } T > T_m \end{cases} \tag{13}$$

The above-mentioned equations used in the current simulation have been applied in previous studies reported by Arshad et al. [14] and Sahoo et al. [48]. They simulated the proposed cases of the PCM–based finned heat sinks, including plate–fin metal structure.

2.3. Initial and boundary conditions

In this study, the initial and boundary conditions are implemented based on previous experimental studies reported by the similar authors [25, 26, 49]. The thermal insulation material are used to isolate the side walls of the heat sink to prevent any heat losses into the surrounding during operation mode. Hence, the boundary of the outer walls are defined as an adiabatic condition, except the surface of the applied heat flux, as labelled in Fig. 1b. Therefore, the initial and boundary conditions used in this study to solve the governing equations can be written as follows:

1. Initial condition:

$$t = 0, T(0) = T_{ini} = 296.15K, f_l = 0$$

2. No–slip boundary conditions at the side walls:

$$u = v = 0$$

3. Adiabatic boundary condition at side wall:

$$\left.\frac{\partial T}{\partial x}\right|_{\substack{x=0-W\\ y=0}} = 0$$

4. Natural convective boundary condition at the top wall:

$$-k\left.\frac{\partial T}{\partial y}\right|_{y=H} = h(T - T_\infty)$$

5. Heat flux supplied at the bottom:

$$-k\left.\frac{\partial T}{\partial y}\right|_{\substack{x=0-W\\ y=0}} = q^{''}$$

2.4. Numerical methodology

The commercial CFD software ANSYS–Fluent 19.1 which coupled the finite volume method with double precision was used to conduct the transient simulation of the proposed configurations in current study. The detailed boundary and initial conditions were indicated for the simulations. Therefore, the energy and momentum equations were discretized using the second-order upwind scheme. The pressure correction equation was solved using the PRESTO scheme, pressure-velocity coupling was captured by SIMPLE (semi–implicit pressure–linked equation) algorithm, and for the momentum and energy equations were adopted by the QUICK (Quadratic Upstream Interpolation for Convective Kinematics) scheme [18, 50]. Melting and solidification model has been used to solve the phase change phenomenon. In particular, the solidification and melting process has been simulated using the enthalpy–porosity method, where the porosity in each cell was adopted to be equal to the liquid fraction in that cell [51]. In addition, the gravity effects were considered in a negative direction of the y–axis. The convergence criteria are set to be 10^{-4}, 10^{-4} and 10^{-6} for continuity, momentum and energy equations, respectively. The accuracy of the numerical improved by carrying out mesh and time independence tests. In the current study, five different mesh sizes with number of elements of 18862, 27126, 42418, 73970 and 167493 were examined. The results of average heat sink temperature, liquid fraction and melting time were compared for each element size reported by the current author mentioned in Ref. [14]. The maximum deviation in average heat sink temperature and melting time and was found to be 0.18% and 1.28%, respectively. Three different time steps of $\Delta t = 0.05$, 0.1 and 0.2 s were investigated for mesh size of 42418 elements and no significant variations were found in liquid-factions, which is because of the low thermal front movement and PCM upfront velocity. Thus, to compromise accuracy and computational cost, a mesh size with 42418 elements and $\Delta t = 0.1$ s time–step were chosen in the current study for further simulations.

2.5. Non–dimensional equations

The non–dimensional numbers are used to normalise the phase transition heat transfer and melting process results of the PCM employed finned heat sinks. To indicate the influence of input power density during the phase change of the PCM inside the finned heat sinks, the non–dimensional heat flux ($\bar{Q}$) is defined as follows [14]:

$$\bar{Q} = \frac{q h_f}{k(T_m - T_{ini})} \tag{14}$$

The average distribution of temperature while heating process of the heat sink is presented with non–dimensional heat temperature (θ) as follows [14]:

$$\theta = \frac{k(T - T_{ini})}{q h_f} \tag{15}$$

To present the transient heat conduction phenomenon, the results are expressed in form of Fourier number (Fo), which is the ratio of the diffusive transport to the stored energy, as follows [14, 38, 45]:

$$Fo = \frac{\alpha t}{h_f^2} \tag{16}$$

Moreover, the natural convective heat transfer distribution in terms of constant heat flux (q) and the temperature difference (ΔT) is expressed in terms of Nusselt number (Nu), as follows [14, 38]:

$$Nu = \frac{q h_f}{\Delta T k} \tag{17}$$

where, (ΔT) is the temperature difference between heat sink base and PCM melting temperature varies with time.

3. Model validation

3.1. With PCM case

The current numerical results are validated with previous published experimental results, reported by Dhaidan et al. [52]. The variations of liquid fraction with time during the melting process of n–Octadecane, which is used as PCM filled in a square cavity, as shown in Fig. 3. The plexiglass made square cavity is used having the dimensions of 25.4×25.4 mm^2 and heated through an electrical heater at Rayleigh number of 2.79×10^8 on the left side and the remaining sides are kept insulated. A good and reasonable agreement is obtained between the present numerical study and the experimental results.

3.2. With fins and PCM case

Another validation of current numerical results is validated with experimental results of the PCM and fin combination reported by Kamkari and Shokouhmand [53], as shown in Fig. 4. A rectangular enclosure with interior of 50 mm in width, 120 mm in height and 120 mm in depth containing 3 fins in vertical direction is selected. The results of melting process are validated through liquid fraction results of lauric acid, used as a PCM, by applying an input wall temperature of 70 °C. A good agreement is obtained between the numerical and experiment results of PCM melting process. The variations in results may be due to radiation and conduction heat transfer and PCM properties varying in experimentation with temperature and time.

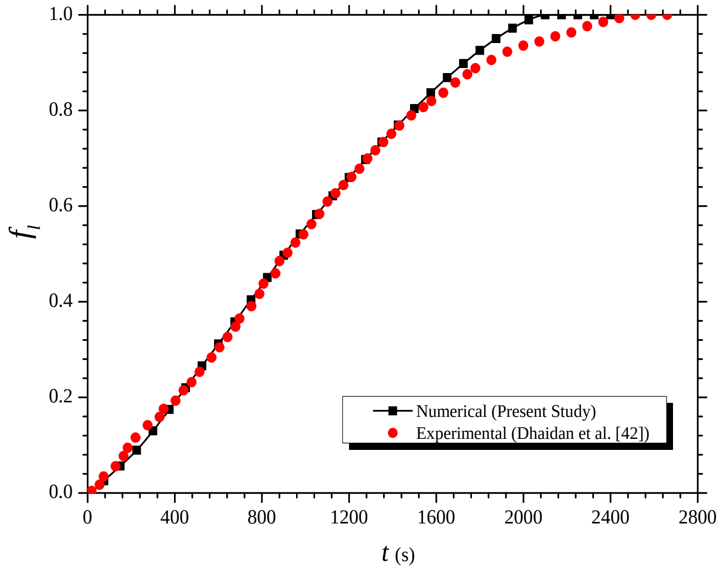

Figure 3: *Validation of present numerical results with experimental results by Dhaidan et al. [52].*

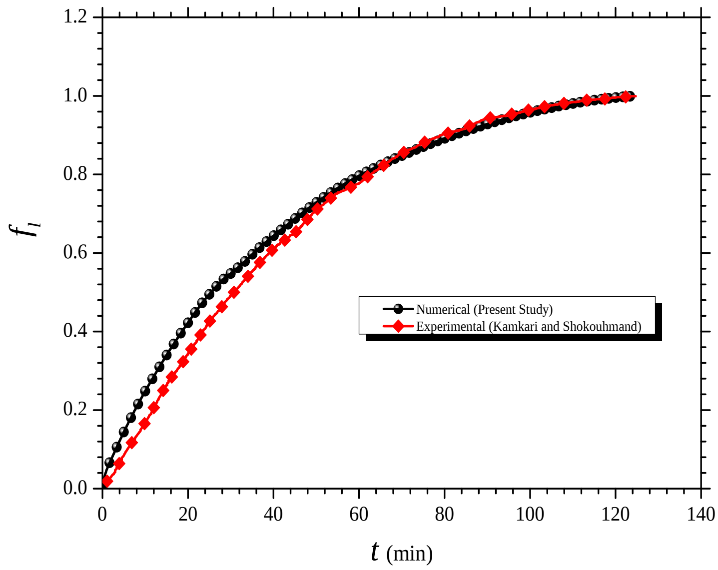

Figure 4: *Validation of present numerical results with experimental results by Kamkari and Shokouhmand [53].*

4. Results and discussion

4.1. Effect of fin height on the heat sink temperature

An analysis of PCM–based heat sinks with no fin and plate-fin with different fin heights and volume fractions are observed. The results are shown for 10% and 20% volume fractions in Fig. 5a and Fig. 5b, respectively. The effect of fin heights is measured to on the basis of the reduction in the heat sink base temperature compared to no fin heat sink filled with PCM. It is evident that the heat sink base temperature in case of no fins remains higher than the base temperature of heat sink with fins of all cases of fin height and reaching a maximum temperature of 363 K during the operation time of 1800 seconds. As expected, the heat sink temperature decreases with increasing fin height. In Fig. 5a, the results indicate that 10 mm plate–fin has the lower effective heat transfer and reached a peak temperature of 361.4 K – a reduction of 0.44% as compared with no fin heat sink at the end of 1800 s timespan. The 15 mm plate–fin is slightly better than the 10 mm case, with a base temperature of 359.7 K and a reduction of 0.91%. The 20 mm plate–fin depicts the best thermal ability, reaching a temperature of 358.4 K with a reduction of 1.3%. A similar comparison can be obtained from Fig. 5b for 20% volume fraction. The maximum temperatures achieved are 360 K and 358 K for 10 mm and 15 mm plate–fin, respectively, with a reduction of 0.83% and 1.3%, respectively. Additionally, the 20 mm plate–fin still prove their thermal ability, reaching a peak temperature of 357.7 K with a reduction of 1.5% as compared with the PCM-based heat sink without fins.

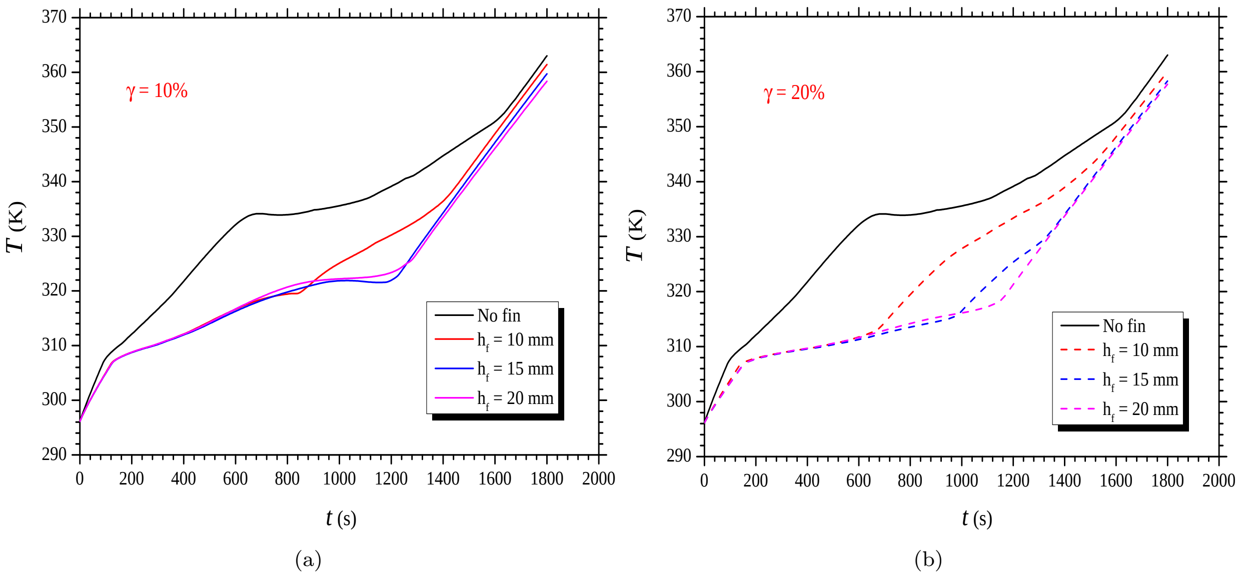

Figure 5: *Temperature-time histories of plate–fin heat sink temperature under various fin heights and constant volume fraction of (a) 10% and (b) 20%.*

4.2. Effect of fin height on melt–fraction of PCM

Fig. 6 shows the liquid fraction of PCM versus time for different plat-fin heights under volume fraction of 10% and 20%, respectively. The results prove that the PCM–based heat sink with no fins requires more time to complete melting compared to that in the finned heat sinks. Furthermore, the results in Figs. 6a and 6b depict that the melting rate increases with higher fin heights. The melting time for the PCM-based heat sink with no fins was found to be 1595 s, whereas the corresponding values for the finned heat sinks under 10%

volume fraction are 1390 s, 1200 s and 1275 s for 10 mm, 15 mm and 20 mm, respectively. In fact, for the 15 mm fin height, the melting rate is higher than 20 mm. This is expected as the uniform distribution of inserted fins leads to uniform heat dissipation into a wide region of PCM. A further investigation can be conducted on the results of liquid fraction versus time for 20% volume fraction as shown in Fig. 6b. The recorded times are 1510 s, 1315 s and 1160 s for 10 mm, 15 mm and 20 mm, respectively. Furthermore, it can be observed from Figs. 6a and 6b that the melting starting time is delayed with increase in fin height. The recorded times are 125 s and 140 s, 130 s and 155 s and 130 s and 155 s for 10% and 20% volume fractions and 10 mm, 15 mm and 20 mm, respectively. It is revealed that a higher fin height contributes to the faster melting rate than a lower fin height because of the more number of fins and more uniformly distribution of heat from heat sink base towards the top surface or ambient.

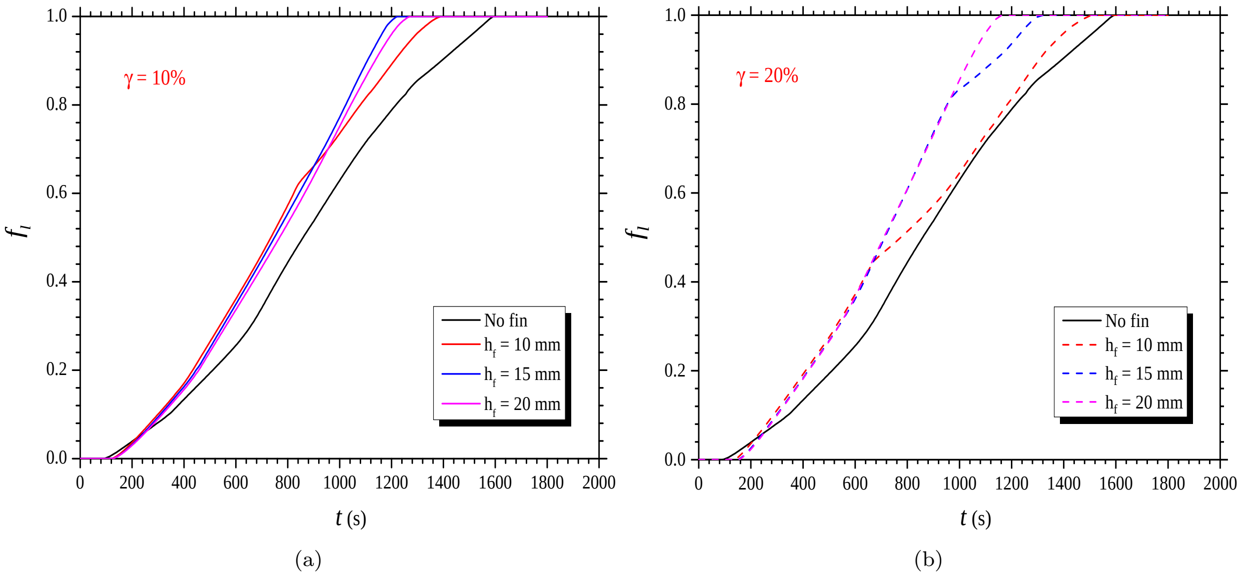

Figure 6: *Melt–fraction curves of plate–fin heat sinks under different fin heights and constant volume fraction of (a) 10% and (b) 20%.*

4.3. Effect of volume fraction on heat sink temperature

Two different percentage levels of volume fractions are chosen to evaluate the effect of fins volume, as shown in Fig. 7. Figs. 7a–7c present a comparison of the heat transfer performance of all heat sink configurations embedded with a PCM including different fins volume fractions of 10% and 20% for 10 mm, 15 mm and 20 mm fin heights, respectively. It is quite essential to evaluate the effect of fins by comparing both the latent–heating phase change and heat sink base temperature. The base temperature of heat sink with no fins has increased rapidly. Furthermore, the results proved that the inserted fins have a significant effect on the thermal performance of the heat sink in term of the reduction of the heat sink base temperature. The 20% volume fraction cases consistently have the better thermal performance than no fins and 10% heat sink in term of keeping the heat sink base temperature under an acceptable level. It is also observed that by increasing the volume fraction, the latent–heating phase will be delayed or increased and therefore has more ability to store energy in the charging phase. This reveals that a heat sink with higher volume fraction of fins has the more tendency to absorb the heat capacity and higher heat transfer capability than lower volume fraction fin heat sink. The lower heat capacity results in a rapid increase in the base temperature. Fig. 7d illustrates the combined results of a temperature–time profile of all simulated configurations. It can be concluded that the 20% volume fraction heat sinks have the best thermal cooling capability as compared to 10% volume fraction heat sinks.

4.4. Effect of volume fractions on melt–fraction of PCM

The impact of volume fraction on the instantaneous liquid fractions of PCM during the melting process for all simulated cases of finned heat sinks with different fin heights are compared in Figs. 8a–8c. The result of no fin heat sink is also presented in the graphs for the purpose of evaluation of the attached fin. As can be seen from Fig. 8a and 8b, at 10 mm and 15 mm, the heat sink with 10% volume fraction always has a higher melting rate compared with 20% volume fraction heat sink. This indicates that $\gamma = 20\%$ is more capable for thermal cooling than $\gamma = 10\%$. Whereas at 20 mm fin height heat sink, the 20% volume fraction has a higher melting rate than 10% volume fraction as shown in Fig. 8c. The reasons for this are that the distribution of the fins inside the heat sink and the distance between two consecutive fins play a key role on the phase change of the PCM. Furthermore, Fig. 8d illustrates a combine comparison of melt–fraction between all investigated cases in this study. It is observed that the 20 mm fin height heat sink at $\gamma = 20\%$ has the higher melting rate compared with all examined configurations.

4.5. Effect of latent–heating phase completion time

The evaluation on thermal performance of plate–fin heat sinks filled with a PCM can be carried out by comparing the completion time of latent-heating phase, as shown in Fig. 9. The latent–heat phase is simply the major aspect for thermal management of electronic devices via PCM-based finned heat sinks. Thus, Fig. 9a presents a comparison of latent-heating phase completion time of different configurations at $\gamma = 10\%$. It is seen that the

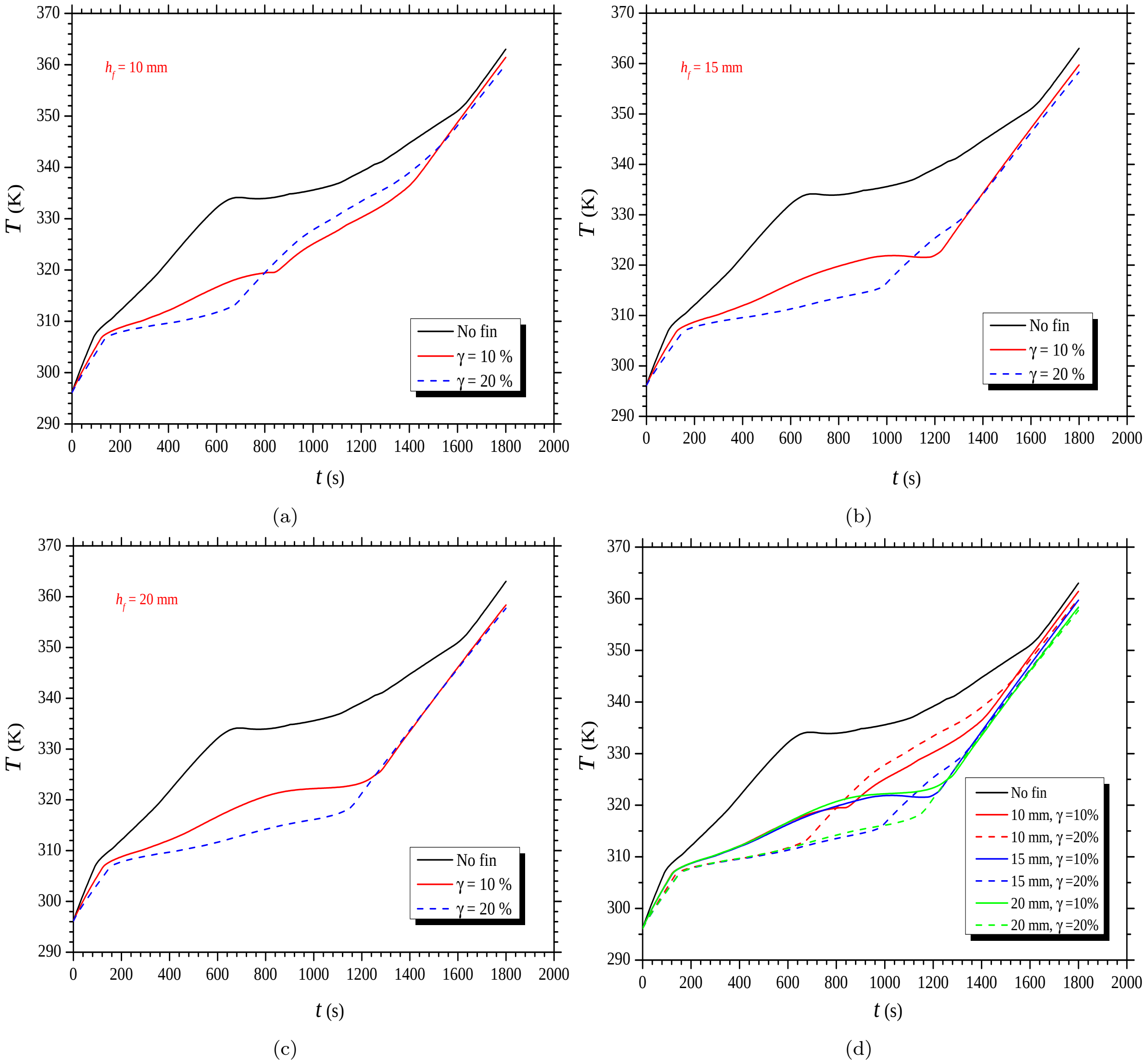

Figure 7: *Time histories of plate–fin heat sink (a) 10 mm, (b) 15 mm, (c) 20 mm under different volume fraction; (d) Time histories of plate-fin heat sink temperature under different fin heights and volume fractions.*

heat sink with no-fins has recoded the longest duration, namely after 1595 s. The reasons are due to the poor thermal conductivity of the embedded PCM and the absence of TCE (e.g., plate–fin) that dissipates the heat uniformly through the PCM. Additionally, a clear picture of 10 mm height plate-fin heat sink indicates a maximum latent-heating phase completion time among other cases. The time achieved was 1390 s compared with 1220 s and 1275 s for 15 mm and 20 mm cases, respectively.

Fig. 9b shows comparison of various configuration at $\gamma = 20\%$. A maximum time of latent–heating completion was achieved by 10 mm fin height case in 1510 s compared with 1315 s and 1160 s for 15 mm and 20 mm cases, respectively. Hence, the optimum number and distribution of fins play a key role to enhance the rate of heat transfer and dissipate the heat

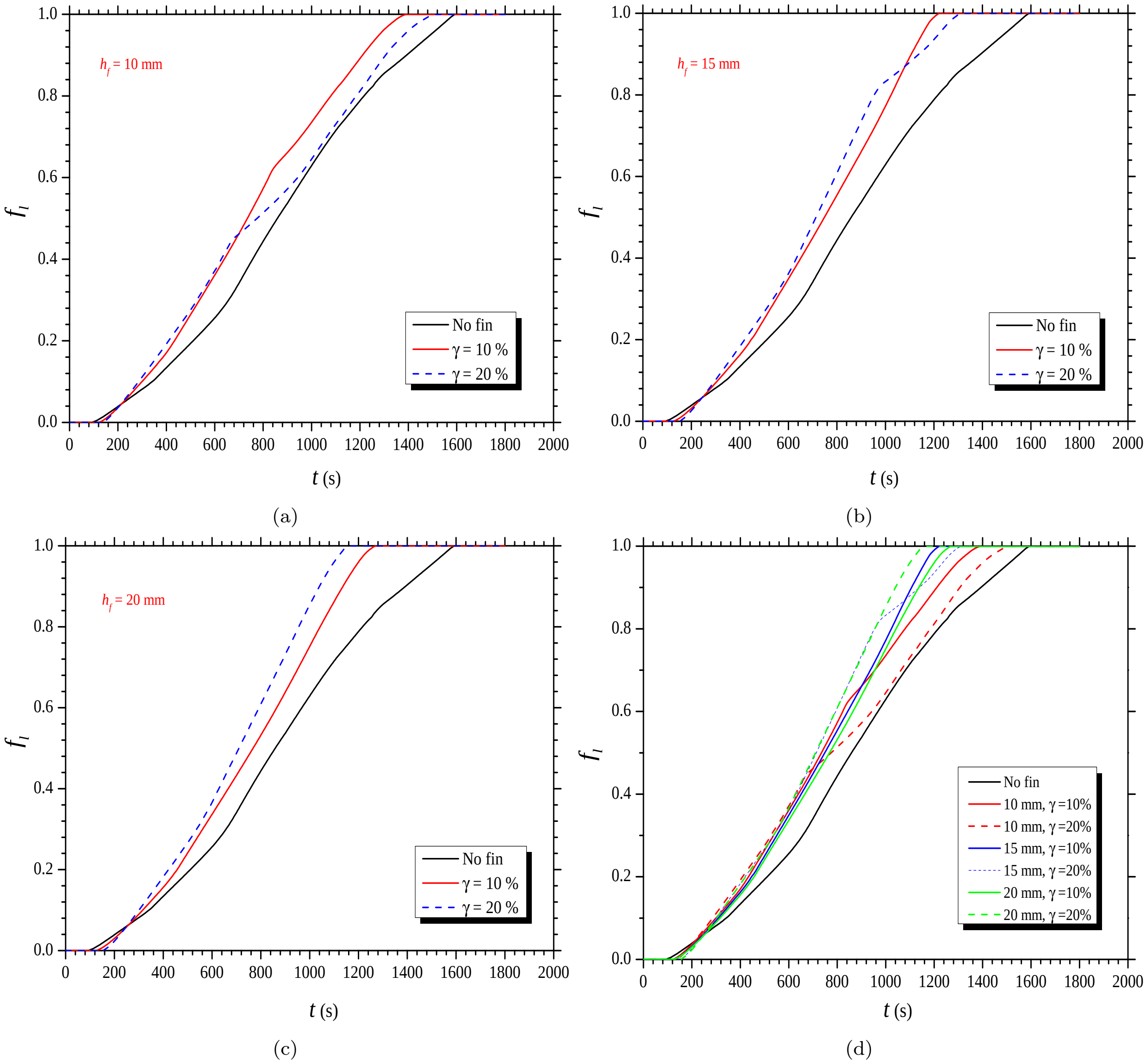

Figure 8: *Time histories of plate–fin heat sink (a) 10 mm, (b) 15 mm, (c) 20 mm under different volume fraction; (d) Time histories of plate-fin heat sink temperature under different fin heights and volume fractions.*

more effectively through the PCM. Therefore, lower thermal conductivity of embedded PCM can be compensated via extended surface geometries (e.g., plate–fins, pin–fins, perforated–fins) that made from high thermal conductivity material and hence, improve the thermal performance of electronics devices.

4.6. Effect of set point temperatures (SPTs)

To ensure the thermal performance of the tested plate–fin heat sinks in this study, the enhancement in operation times of three critical SPTs of 40 °C, 45 °C and 50 °C are chosen for analysis at two volume fractions of TCE. Bar charts shown in Fig. 10a and Fig. 10b depict the time taken by the unfinned and finned heat sinks against different fin heights to

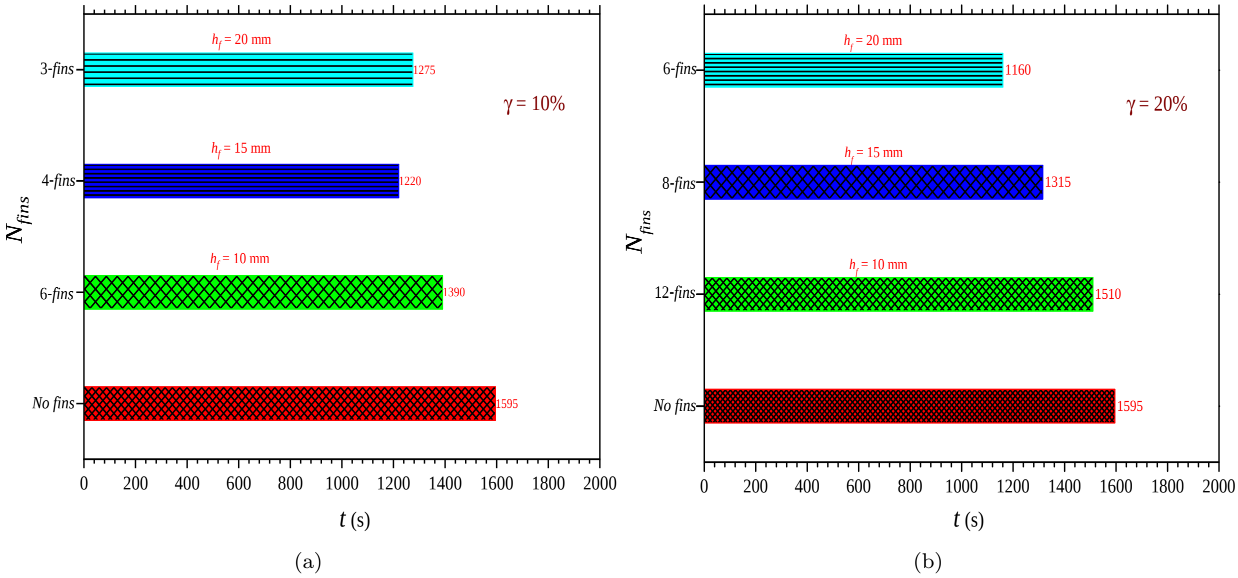

Figure 9: *Comparison of enhancement time between various configuration of plate-fin heat sinks under different fin height and constant γ of (a) 10% and (b) 20%.*

reach the SPTs for $\gamma = 10\%$ and $\gamma = 20\%$, respectively. Fig. 10a reveals that it takes lower time for unfinned heat sink to reach SPTs of 40 °C, 45 °C, and 50 °C; the reported times are 3.75 min, 5.60 min and 7.10 min, respectively. This is expected due to the absence of the fins. Moreover, the 15 mm fin height heat sink takes more time in comparison to other tested configurations. The maximum time of 7.75 min, 11.60 min and 20.60 min are noted for 15 mm fin height case to reach SPTs of 40 °C, 45 °C, and 50 °C, respectively.
Fig. 10b shows a similar comparison at $\gamma = 20\%$. It is evident that operation time increases linearly as the fin height increases for a specific SPT. For instance, it takes 12.90 min to reach a SPT of 45 °C for 10 mm fin heat sink, whereas it is 17.25 min and 19.10 min for 15 mm and 20 fin height cases, respectively. A closer look reveals that it takes 7.50 min to reach a SPT of 40 °C for 10 mm fin height heat sink at $\gamma = 10\%$. In contrast, it takes 11.25 min to reach the same SPT and fin height heat sink at $\gamma = 20\%$. Therefore, as the volume fraction of fins increases the time duration increases to reach a specific SPT.

4.7. Effect of volume fraction on average heat sink temperature

Fig. 11a and Fig. 11b show an analysis on the role of γ in thermal management of electronic devices at γ of 10% and 20%, respectively. The average temperature of the unfinned and finned heat sinks is calculated at a specific time.

$$T = \frac{1}{t_i - t_f} \int_{t_f}^{t_i} T_{t_i} dt \tag{18}$$

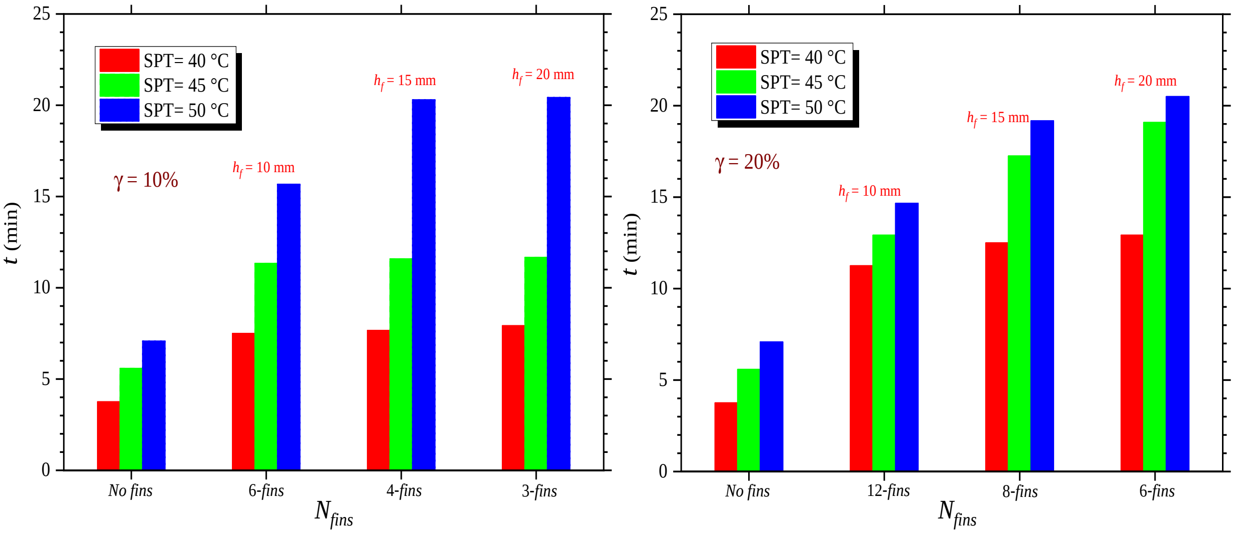

(a) (b)

Figure 10: *Enhancement in operation time for different critical STPs under different fin heights and constant volume fraction of (a) 10% and (b) 20%.*

The average temperature at each fin height heat sinks at $\gamma = 10\%$ are illustrated as bar charts in Fig. 11a. The unfinned heat sink has recorded the highest average temperature among the other configurations and reached a peak of 89.90 °C. Whereas in the finned heat sink cases, the average temperature decreases as the fin height increases. At fin height of 10 mm, the average temperature was 88.30 °C – a decrease of 1.8% compared with unfinned heat sinks, while the temperature has decreased gradually for 15 mm and 20 mm fin height heat sinks and record a temperature of 86.60 °C and 85.20 °C – a decrease of 3.7% and 5.2%, respectively.

Fig. 11b shows a similar comparison at $\gamma = 20\%$. The average temperature at fin height of 10 mm, 15 mm and 20 mm was 86.90 °C, 85.20 °C and 84.60 °C – a decrease of 1.6%, 1.6% and 0.7%, respectively, as compared with the same configurations at $\gamma = 10\%$. This reveals that the fins play a key role to enhance the rate of heat transfer inside the heat sink and keep the base temperature under an acceptable temperature. Furthermore, the PCM absorbs and stores the excess heat in the form of thermal energy (as latent–heat of fusion) at nearly constant temperature. Hence, the average temperature of the heat sinks will be kept within an accepted level.

4.8. Effects of dimensionless parameters

Fig. 12 shows the variation of dimensionless average heat sink temperature (θ), liquid fraction (f_l) and Nusselt number (Nu) in terms of Fourier number (Fo) for different fin heights of 10 mm, 15 mm, and 20 mm at constant dimensionless heat fluxes ($\bar{Q}$ = 17, 25

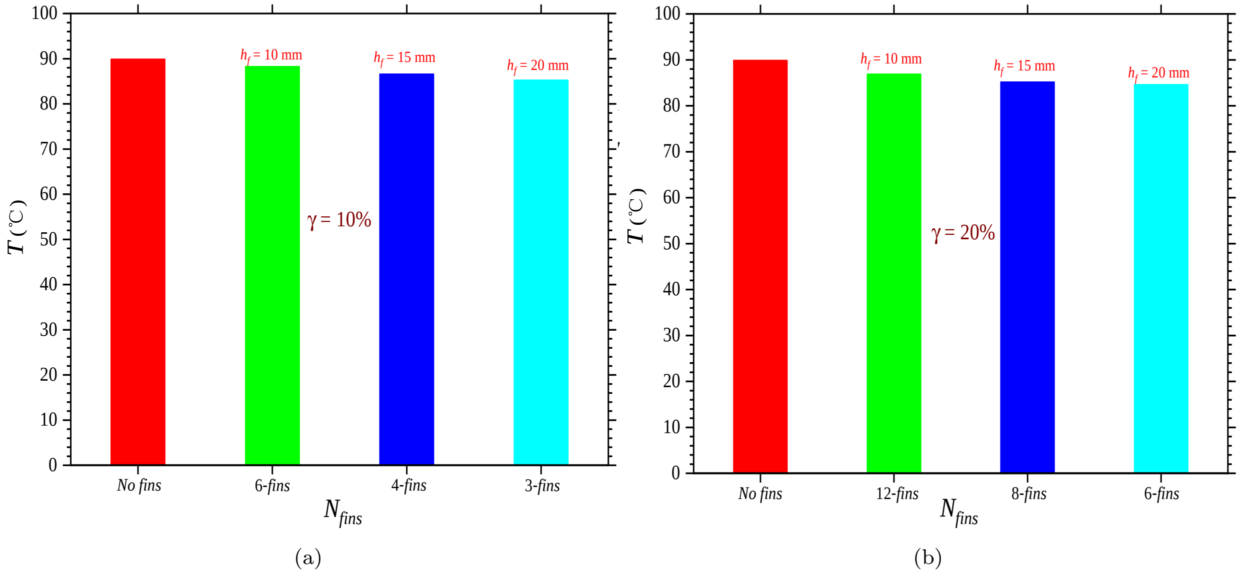

Figure 11: *Comparison between average temperature of no fin heat sink and finned heat sinks under various fin heights and constant γ of (a) 10% and (b) 20%.*

and 34), respectively. At $\bar{Q} = 25$ and 34, the variation in θ of PCM–based heat sink firstly reflects a gradual increase in temperature during the phase change process of PCM with the rise in Fo, followed by a sharp increase in temperature, as shown in Fig. 12a. At constant $\bar{Q}$, the $\gamma = 10\%$ and $\gamma = 20\%$ have a slight difference in temperature for all fin heights. However, the $\gamma = 20\%$ heat sinks always record lower θ, which indicates better thermal performance of heat sink due to increase in phase transition duration of PCM from solid to liquid. Furthermore, during the melting process, θ is higher for a higher $\bar{Q}$. The melting of PCM is completed in a lower Fo for a higher $\bar{Q}$ as shown in Fig. 12a. By increasing the fin height, the $\bar{Q}$ increased, and therefore, Fo decreases and θ increased. Fig. 12b illustrates the distribution of f_l as a function of Fo for PCM–based heat sink at fin heights of 10 mm, 15 mm, and 20 mm at $\gamma = 10\%$ and $\gamma = 20\%$. For lower to higher fin heights (i.e. 10 to 20 mm) or lower to higher $\bar{Q}$ (i.e. 17–34), the rate of f_l increases with the decrease of Fo which shows the increasing the fin height of a PCM based heat sink enhances the melting rate of PCM. Further effects of heat transfer effects under natural heat convection are presented in terms of Nu and Fo in Fig. 12c. A steep reduction in Nu is observed with the increase of Fo for all $\bar{Q}$. Initially , the higher Nu is obtained of melting process which is because of the less thermal resistance. However, a sharp decline is observed as the f_l is obtained about 0.2–0.4 and further decreases asymptotically approaching a non–zero value representing a natural convection heat transfer while fulling melting of PCM.

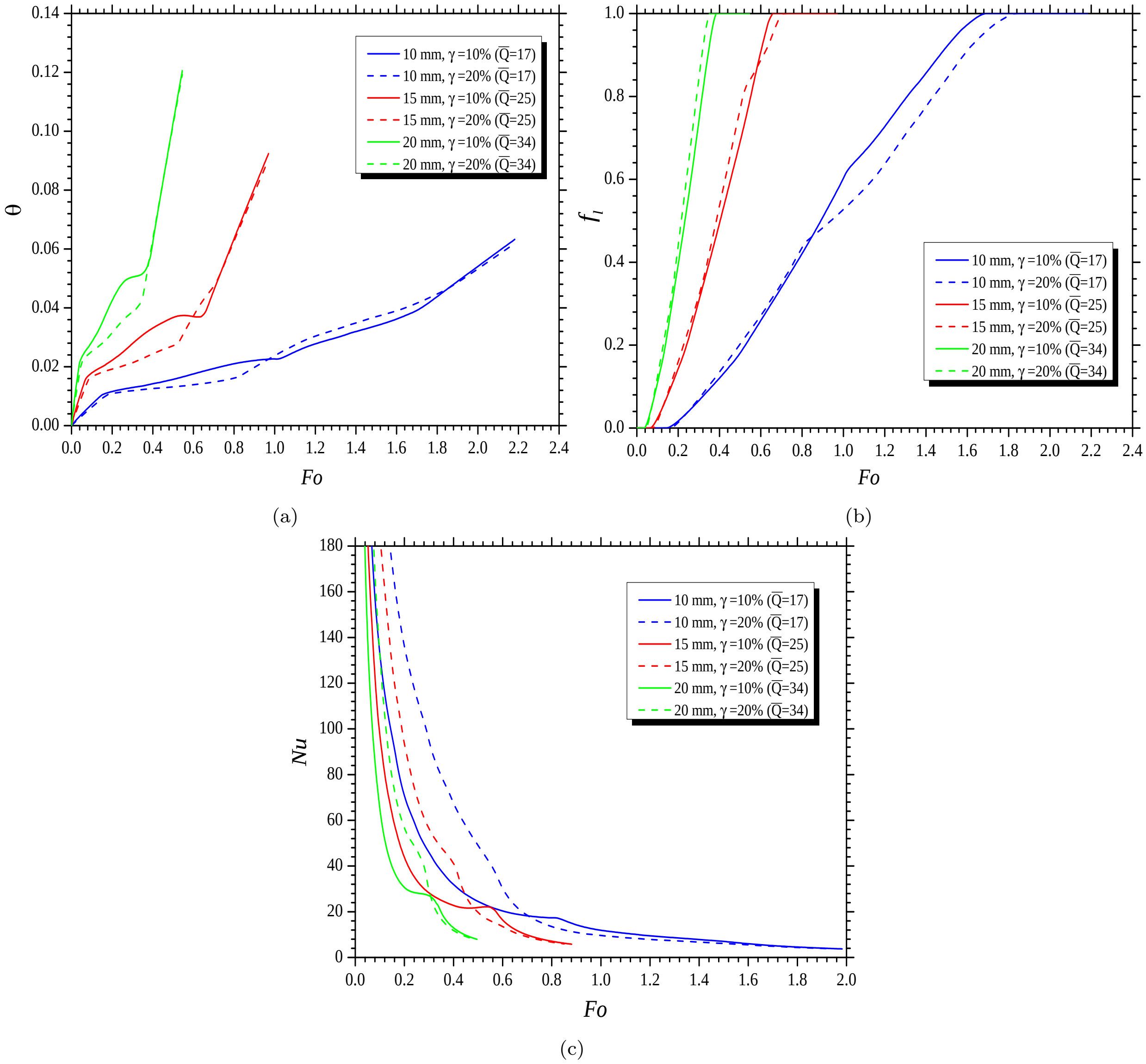

Figure 12: *(a) The variation of θ in terms of Fo, (b) The variation of f_l in terms of Fo, (c) The variation of Nu in terms of Fo under various fin heights and volume fractions.*

4.9. Evaluation of isotherm and liquid fraction

Fig. 13 illustrates the rates of heat transfer and temperature distribution of no fin heat sink and 20 mm fin height heat sinks at $\gamma = 10\%$ and $\gamma = 20\%$ embedded with a PCM. It can be seen clearly that the rate of temperature increase is higher in $\gamma = 10\%$ heat sink as compared to $\gamma = 20\%$ heat sink at each time step. For instance, the temperature varies from 356.5 K to 358.4 K for $\gamma = 10\%$ heat sink at 30 min, whereas it varies from 355.9 K to 357.7 K for $\gamma = 20\%$ heat sink at the same time. The reason is due to the optimum number and distribution of fins in $\gamma = 20\%$ heat sink as compared to the $\gamma = 10\%$ heat sink. In addition, the heat diffusion in the PCM region is relatively more in $\gamma = 20\%$ heat sink resulting in more heat absorbed from the base of the heat sink and keeping the temperature at an acceptable level, as showing in Fig. 13 especially at time 15 min.

An additional comparison of liquid fraction contours for the same configurations are shown in Fig. 14. The PCM-based heat sink of $\gamma = 20\%$ has a higher PCM melting rate as compared to $\gamma = 10\%$ heat sink. This is due to the more number of fins which led to an optimum distribution of fins and heat transfer area. The higher PCM melting rate of $\gamma = 20\%$ heat sink enhances the heat absorption and transfer into the surrounding, leading to more capable thermal cooling.

5. Conclusions

The present numerical study explores the parametric investigation of a PCM–based plate–fin heat sinks by exploring the different fin heights of 10, 15 and 20 mm for two different volume fractions of 10% and 20% of fins under a constant input power level. The heat transfer, melting and temperature flow–field characteristics. Further, the results of dimensionless numbers provided the further generalized relationship between the fin height and number of fins for both volume fractions of fin heat sinks to analyse the natural heat transfer and passive cooling performance of PCM filled plate-fin heat sink. The results revealed that addition of metal fins reduced the average temperature of the heat sink base by extracting the heat from base towards the ambient. Further, the addition of fins improved the melting of PCM uniformly and more uniform melting is obtained at the fin height of 20 mm and volume fraction of 20% which is because of the higher number of fins. The maximum reduction in heat sink base temperature was obtained of 1.5% with 20 mm fin height and 20% volume fraction. However, a PCM filled heat sink of 10% volume fraction with 20 mm fin height reduced the base temperature at an acceptable level. The melting time of PCM was delayed with the increase of fin height for both volume fractions which is because of the higher specific heat capacity at higher fin height than a lower fin height. In addition, increasing the volume fraction of fins also delayed the latent-heating phase which revealed to store more thermal energy during charging phase. The melting time is reduced with the increase of number of fins for volume fractions of 10% and 20%. Moreover, the 20% volume fraction of PCM based finned heat sink revealed the less melting time corresponding each fin height of 10% volume fraction PCM based finned heat sink. The higher operating time was obtained with the increase of SPT against at a certain fin height for both 10% and 20% volume fraction of fins PCM based heat sink. The lower heat sink temperature is obtained at 20 mm fin height either for 10% volume fraction or 20%. Thus, it is highly

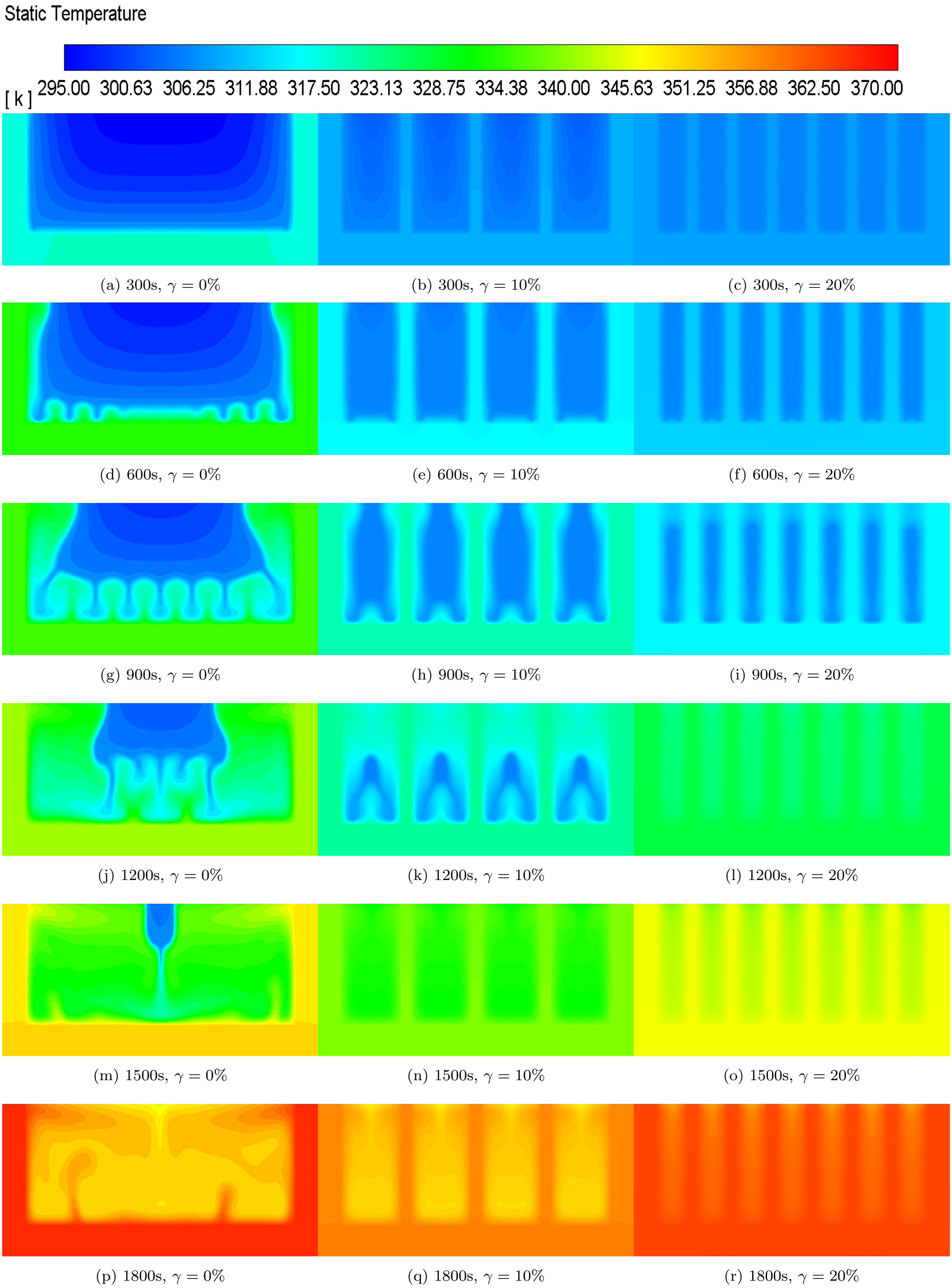

Figure 13: *Comparison of isotherms contours at various time period of PCM filled heat sink at volume fractions of 0%, 10% and 20%.*

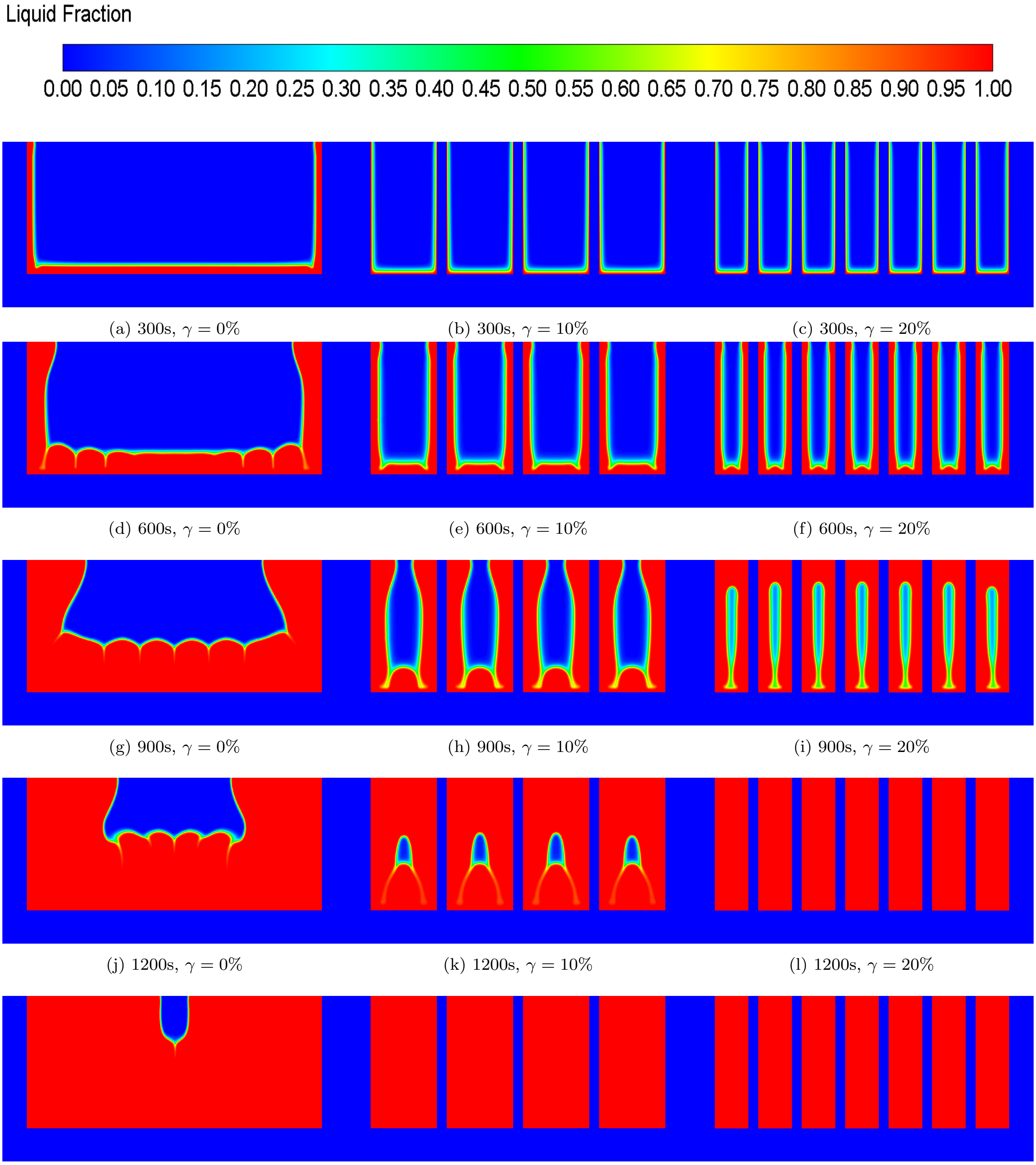

(a) 300s, $\gamma = 0\%$ (b) 300s, $\gamma = 10\%$ (c) 300s, $\gamma = 20\%$

(d) 600s, $\gamma = 0\%$ (e) 600s, $\gamma = 10\%$ (f) 600s, $\gamma = 20\%$

(g) 900s, $\gamma = 0\%$ (h) 900s, $\gamma = 10\%$ (i) 900s, $\gamma = 20\%$

(j) 1200s, $\gamma = 0\%$ (k) 1200s, $\gamma = 10\%$ (l) 1200s, $\gamma = 20\%$

(m) 1500s, $\gamma = 0\%$ (n) 1500s, $\gamma = 10\%$ (o) 1500s, $\gamma = 20\%$

Figure 14: *Comparison of liquid fraction contours at various time period of PCM filled heat sink at volume fractions of 0%, 10% and 20%.*

recommended that a PCM based heat sink with 20 mm or equal to the height of PCM has the better thermal storage and heat transfer performance. The results of isotherm and melting fraction showed that the uniform melting of PCM was obtained with the addition of fins under the natural heat transfer convection and gravitational effects. Moreover, the results of Nusselt number revealed that 20 mm fin height of 10% or 20% volume fraction of fins had lower Fourier number which shows the higher effects of natural convection inside the heat sink. Thus, it is recommended that a heat sink of 20 mm height of 10% volume fraction of fins filled with PCM is the preferable for passive cooling of electronic devices.

Acknowledgement

This research is facilitated by the Faculty of Engineering, University of Nottingham, UK research infrastructure. The corresponding author (Adeel Arshad) acknowledges the University of Nottingham for awarding him the *Faculty of Engineering Research Excellence PhD Scholarship* to pursue a Ph.D. research program.

Conflict of interest

The authors declare no conflict of interest regarding this research article.

References

[1] S.M. Sohel Murshed and C.A. Nieto de Castro. A critical review of traditional and emerging techniques and fluids for electronics cooling. *Renewable and Sustainable Energy Reviews*, 78:821–833, oct 2017.

[2] Saad Mahmoud, Aaron Tang, Chin Toh, Raya AL-Dadah, and Sein Leung Soo. Experimental investigation of inserts configurations and PCM type on the thermal performance of PCM based heat sinks. *Applied Energy*, 112:1349–1356, dec 2013.

[3] Ronan Grimes, Ed Walsh, and Pat Walsh. Active cooling of a mobile phone handset. *Applied Thermal Engineering*, 30(16):2363–2369, nov 2010.

[4] Kh. Hosseinzadeh, M.A. Erfani Moghaddam, A. Asadi, A.R. Mogharrebi, and D.D. Ganji. Effect of internal fins along with hybrid nano-particles on solid process in star shape triplex latent heat thermal energy storage system by numerical simulation. *Renewable Energy*, 154:497–507, jul 2020.

[5] Kh. Hosseinzadeh, M.A. Erfani Moghaddam, A. Asadi, A.R. Mogharrebi, B. Jafari, M.R. Hasani, and D.D. Ganji. Effect of two different fins (longitudinal-tree like) and hybrid nano-particles (MoS2-TiO2) on solidification process in triplex latent heat thermal energy storage system. *Alexandria Engineering Journal*, 60(1):1967–1979, feb 2021.

[6] Kh. Hosseinzadeh, Elham Montazer, Mohammad Behshad Shafii, and A.R.D. Ganji. Solidification enhancement in triplex thermal energy storage system via triplets fins configuration and hybrid nanoparticles. *Journal of Energy Storage*, 34:102177, feb 2021.

[7] Adeel Arshad, Mark Jabbal, and Yuying Yan. Thermal performance of PCM-based heat sink with partially filled copper oxide coated metal-foam for thermal management of microelectronics. In *2020 19th IEEE Intersociety Conference on Thermal and Thermomechanical Phenomena in Electronic Systems (ITherm)*. IEEE, jul 2020.

[8] Qinlong Ren, Zexiao Wang, Jianjun Zhu, and Z.G. Qu. Pore-scale heat transfer of heat sink filled with stacked 2d metal fiber-PCM composite. *International Journal of Thermal Sciences*, 161:106739, mar 2021.

[9] Qinlong Ren, Zexiao Wang, Tao Lai, J.F. Zhang, and Z.G. Qu. Conjugate heat transfer in anisotropic woven metal fiber-phase change material composite. *Applied Thermal Engineering*, 189:116618, may 2021.

[10] Qinlong Ren, Penghua Guo, and Jianjun Zhu. Thermal management of electronic devices using pin-fin based cascade microencapsulated PCM/expanded graphite composite. *International Journal of Heat and Mass Transfer*, 149:119199, mar 2020.

[11] Z.G. Qu, W.Q. Li, and W.Q. Tao. Numerical model of the passive thermal management system for high-power lithium ion battery by using porous metal foam saturated with phase change material. *International Journal of Hydrogen Energy*, 39(8):3904–3913, mar 2014.

[12] R. Srikanth and C. Balaji. Experimental investigation on the heat transfer performance of a PCM based pin fin heat sink with discrete heating. *International Journal of Thermal Sciences*, 111:188–203, jan 2017.

[13] Santosh Kumar Sahoo, Mihir Kumar Das, and Prasenjit Rath. Application of TCE-PCM based heat sinks for cooling of electronic components: A review. *Renewable and Sustainable Energy Reviews*, 59:550–582, jun 2016.

[14] Adeel Arshad, Mark Jabbal, Pouyan Talebizadeh Sardari, Muhammad Anser Bashir, Hamza Faraji, and Yuying Yan. Transient simulation of finned heat sinks embedded with PCM for electronics cooling. *Thermal Science and Engineering Progress*, 18:100520, aug 2020.

[15] Hassan Nazir, Mariah Batool, Francisco J. Bolivar Osorio, Marllory Isaza-Ruiz, Xinhai Xu, K. Vignarooban, Patrick Phelan, Inamuddin, and Arunachala M. Kannan. Recent developments in phase change materials for energy storage applications: A review. *International Journal of Heat and Mass Transfer*, 129:491–523, feb 2019.

[16] Nidal H. Abu-Hamdeh and Khaled A. Alnefaie. Assessment of thermal performance of PCM in latent heat storage system for different applications. *Solar Energy*, 177:317–323, jan 2019.

[17] Jose Pereira da Cunha and Philip Eames. Thermal energy storage for low and medium temperature applications using phase change materials – a review. *Applied Energy*, 177:227–238, sep 2016.

[18] Rajesh Akula and C. Balaji. Thermal performance of a phase change material-based heat sink subject to constant and power surge heat loads: A numerical study. *Journal of Thermal Science and Engineering Applications*, 13(3), sep 2020.

[19] Adeel Arshad, Hafiz Muhammad Ali, Wei-Mon Yan, Ahmed Kadhim Hussein, and Majid Ahmadlouydarab. An experimental study of enhanced heat sinks for thermal management using n-eicosane as phase change material. *Applied Thermal Engineering*, 132:52–66, mar 2018.

[20] Harald Mehling and Luisa F. Cabeza. PHASE CHANGE MATERIALS AND THEIR BASIC PROPERTIES. In *NATO Science Series*, pages 257–277. Springer Netherlands.

[21] Zhaolin Gu, Hongjuan Liu, and Yun Li. Thermal energy recovery of air conditioning system—heat recovery system calculation and phase change materials development. *Applied Thermal Engineering*, 24(17-18):2511–2526, dec 2004.

[22] Theodore D. Swanson and Gajanana C. Birur. NASA thermal control technologies for robotic spacecraft. *Applied Thermal Engineering*, 23(9):1055–1065, jun 2003.

[23] Mahmud M. Alkilani, K. Sopian, M.A. Alghoul, M. Sohif, and M.H. Ruslan. Review of solar air collectors with thermal storage units. *Renewable and Sustainable Energy Reviews*, 15(3):1476–1490, apr 2011.

[24] T. Arunkumar, D. Denkenberger, Amimul Ahsan, and R. Jayaprakash. The augmentation of distillate yield by using concentrator coupled solar still with phase change material. *Desalination*, 314:189–192, apr 2013.

[25] Hafiz Muhammad Ali and Adeel Arshad. Experimental investigation of n-eicosane based circular pin-fin heat sinks for passive cooling of electronic devices. *International Journal of Heat and Mass Transfer*, 112:649–661, sep 2017.

[26] Hafiz Muhammad Ali, Adeel Arshad, Muhammad Mansoor Janjua, Wajahat Baig, and Uzair Sajjad. Thermal performance of LHSU for electronics under steady and transient operations modes. *International Journal of Heat and Mass Transfer*, 127:1223–1232, dec 2018.

[27] X. Duan and G.F. Naterer. Heat transfer in phase change materials for thermal management of electric vehicle battery modules. *International Journal of Heat and Mass Transfer*, 53(23-24):5176–5182, nov 2010.

[28] A Mahrous. Thermal performance of pcm based heat sinks. *International Journal of Mechanical Engineering*, 2(4), 2013.

[29] K.C. Nayak, S.K. Saha, K. Srinivasan, and P. Dutta. A numerical model for heat sinks with phase change materials and thermal conductivity enhancers. *International Journal of Heat and Mass Transfer*, 49(11-12):1833–1844, jun 2006.

[30] Adeel Arshad, Hafiz Muhammad Ali, Shahab Khushnood, and Mark Jabbal. Experimental investigation of PCM based round pin-fin heat sinks for thermal management of electronics: Effect of pin-fin diameter. *International Journal of Heat and Mass Transfer*, 117:861–872, feb 2018.

[31] Mustafa Yusuf Yazici, Mete Avci, and Orhan Aydin. Combined effects of inclination angle and fin number on thermal performance of a PCM-based heat sink. *Applied Thermal Engineering*, 159:113956, aug 2019.

[32] Jinlong Xie, Kok Fah Choo, Jianhua Xiang, and Hsiao Mun Lee. Characterization of natural convection in a PCM-based heat sink with novel conductive structures. *International Communications in Heat and Mass Transfer*, 108:104306, nov 2019.

[33] A. ABHAT. Experimental investigation and analysis of a honeycomb-packed phase change material device. In *11th Thermophysics Conference*. American Institute of Aeronautics and Astronautics, jul 1976.

[34] Muhammad Junaid Ashraf, Hafiz Muhammad Ali, Hazrat Usman, and Adeel Arshad. Experimental passive electronics cooling: Parametric investigation of pin-fin geometries and efficient phase change materials. *International Journal of Heat and Mass Transfer*, 115:251–263, dec 2017.

[35] Rasool Kalbasi. Introducing a novel heat sink comprising PCM and air - adapted to electronic device thermal management. *International Journal of Heat and Mass Transfer*, 169:120914, apr 2021.

[36] S.C. Fok, W. Shen, and F.L. Tan. Cooling of portable hand-held electronic devices using phase change materials in finned heat sinks. *International Journal of Thermal Sciences*, 49(1):109–117, jan 2010.

[37] Yi-Hsien Wang and Yue-Tzu Yang. Three-dimensional transient cooling simulations of a portable electronic device using PCM (phase change materials) in multi-fin heat sink. *Energy*, 36(8):5214–5224, aug 2011.

[38] V. Shatikian, G. Ziskind, and R. Letan. Numerical investigation of a PCM-based heat sink with internal fins. *International Journal of Heat and Mass Transfer*, 48(17):3689–3706, aug 2005.

[39] V. Shatikian, G. Ziskind, and R. Letan. Numerical investigation of a PCM-based heat sink with internal fins: Constant heat flux. *International Journal of Heat and Mass Transfer*, 51(5-6):1488–1493, mar 2008.

[40] R. Pakrouh, M.J. Hosseini, A.A. Ranjbar, and R. Bahrampoury. A numerical method for PCM-based pin fin heat sinks optimization. *Energy Conversion and Management*, 103:542–552, oct 2015.

[41] S.F. Hosseinizadeh, F.L. Tan, and S.M. Moosania. Experimental and numerical studies on performance of PCM-based heat sink with different configurations of internal fins. *Applied Thermal Engineering*, 31(17-18):3827–3838, dec 2011.

[42] Hafiz Muhammad Ali, Muhammad Junaid Ashraf, Ambra Giovannelli, Muhammad Irfan, Talal Bin Irshad, Hafiz Muhammad Hamid, Faisal Hassan, and Adeel Arshad. Thermal management of electronics: An experimental analysis of triangular, rectangular and circular pin-fin heat sinks for various PCMs. *International Journal of Heat and Mass Transfer*, 123:272–284, aug 2018.

[43] Adeel Arshad, Mark Jabbal, Lei Shi, Jo Darkwa, Nicola J. Weston, and Yuying Yan. Development of TiO2/RT–35hc based nanocomposite phase change materials (NCPCMs) for thermal management applications. *Sustainable Energy Technologies and Assessments*, 43:100865, feb 2021.

[44] Adeel Arshad, Mark Jabbal, Hamza Faraji, Muhammad Anser Bashir, Pouyan Talebizadehsardari, and Yuying Yan. Thermal process enhancement of HNCPCM filled

heat sink: Effect of hybrid nanoparticles ratio and shape. *International Communications in Heat and Mass Transfer*, 125:105323, jun 2021.

[45] S.K. Saha and P. Dutta. Heat transfer correlations for PCM-based heat sinks with plate fins. *Applied Thermal Engineering*, 30(16):2485–2491, nov 2010.

[46] Adeel Arshad, Mark Jabbal, Hamza Faraji, Pouyan Talebizadehsardari, Muhammad Anser Bashir, and Yuying Yan. Numerical study of nanocomposite phase change material-based heat sink for the passive cooling of electronic components. *Heat and Mass Transfer*, may 2021.

[47] Huizhu Yang, Yongyao Li, Liang Zhang, and Yonggang Zhu. Thermal performance enhancement of phase change material heat sinks for thermal management of electronic devices under constant and intermittent power loads. *International Journal of Heat and Mass Transfer*, 181:121899, dec 2021.

[48] Santosh Kumar Sahoo, Prasenjit Rath, and Mihir Kumar Das. Numerical study of phase change material based orthotropic heat sink for thermal management of electronics components. *International Journal of Heat and Mass Transfer*, 103:855–867, dec 2016.

[49] Hafiz Muhammad Ali, Adeel Arshad, Mark Jabbal, and P.G. Verdin. Thermal management of electronics devices with PCMs filled pin-fin heat sinks: A comparison. *International Journal of Heat and Mass Transfer*, 117:1199–1204, feb 2018.

[50] Suhas Patankar. *Numerical heat transfer and fluid flow.* Hemisphere Publishing Corporation; McGraw-Hill Book Company, New York., 2018.

[51] A. D. Brent, V. R. Voller, and K. J. Reid. Enthalpy-porosity technique for modeling convection-diffusion phase change: application to the melting of a pure metal. *Numerical Heat Transfer*, 13(3):297–318, apr 1988.

[52] Nabeel S. Dhaidan, J.M. Khodadadi, Tahseen A. Al-Hattab, and Saad M. Al-Mashat. Experimental and numerical investigation of melting of phase change material/nanoparticle suspensions in a square container subjected to a constant heat flux. *International Journal of Heat and Mass Transfer*, 66:672–683, nov 2013.

[53] Babak Kamkari and Hossein Shokouhmand. Experimental investigation of phase change material melting in rectangular enclosures with horizontal partial fins. *International Journal of Heat and Mass Transfer*, 78:839–851, nov 2014.